Supporting information

Role of Zn in enhancing CO_2 hydrogenation to methanol over Zn_xZrO_y catalysts

Zinat Zanganeh [a], Max Bols [a], Parviz Yazdani [a], Hilde Poelman [a], and Mark Saeys *[a]

[a] *Laboratory for Chemical Technology, Ghent University, Technologiepark 125, B-9052 Gent, Belgium.*

* *Corresponding author: mark.saeys@ugent.be*

Section 1. SEM-EDX

Table S1. Catalysts' composition measured by SEM-EDX.

	wt.%	ZrO_2	$Zn_{0.01}ZrO_y$-500	$Zn_{0.07}ZrO_y$-500	$Zn_{0.19}ZrO_y$-500	$Zn_{0.28}ZrO_y$-500	$Zn_{0.44}ZrO_y$-500	$Zn_{0.56}ZrO_y$-500	$Zn_{0.19}ZrO_y$-550	$Zn_{0.19}ZrO_y$-700	$Zn_{0.19}ZrO_y$-800
a*	Zn	---	1.19	5.54	11.52	14.77	35.19	37.77	11.36	10.67	9.76
	Zr	40.46	48.44	44.25	33.35	29.53	25.94	20.56	41.25	40.11	41.42
	O	59.54	50.37	50.21	55.13	55.7	38.87	41.67	47.38	49.22	48.82
	Zn/Zr	---	0.02	0.13	0.35	0.50	1.36	1.84	0.28	0.27	0.24
b*	Zn	---	0.25	4.12	8.75	11.58	27.81	31.63	9.16	8.1	7.15
	Zr	62.21	67.98	64.6	53.55	50.43	44.83	36.64	60.7	60.79	61.89
	O	37.79	31.78	31.27	37.7	37.99	27.36	31.73	30.14	31.11	30.96
	Zn/Zr	---	0.00	0.06	0.16	0.23	0.62	0.86	0.15	0.13	0.12
c*	Zn	---	0.15	3.25	7.31	10.71	23.74	28.71	7.57	6.79	6.19
	Zr	73.17	78.27	74.81	64.58	60.3	55.08	46.73	70.13	70.5	71.08
	O	26.83	21.58	21.94	28.11	28.99	21.18	24.56	22.3	22.71	22.73
	Zn/Zr	---	0.00	0.04	0.11	0.18	0.43	0.61	0.11	0.10	0.09
d*	Zn	---	2.09	2.64	6.74	9.42	21.1	25.33	6.39	5.92	5.39
	Zr	79.82	61.8	80.1	71.21	66.79	61.31	53.28	76.14	75.87	77.15
	O	20.18	36.12	17.26	22.05	23.8	17.59	21.39	17.47	18.21	17.46
	Zn/Zr	---	0.03	0.03	0.09	0.14	0.34	0.48	0.08	0.08	0.07

	Atomic %	ZrO_2	$Zn_{0.01}ZrO_y$-500	$Zn_{0.07}ZrO_y$-500	$Zn_{0.19}ZrO_y$-500	$Zn_{0.28}ZrO_y$-500	$Zn_{0.44}ZrO_y$-500	$Zn_{0.56}ZrO_y$-500	$Zn_{0.19}ZrO_y$-550	$Zn_{0.19}ZrO_y$-700	$Zn_{0.19}ZrO_y$-800
a*	Zn	---	0.49	2.28	4.42	5.61	16.55	16.96	4.85	4.43	4.09
	Zr	10.65	14.36	13.08	9.17	8.03	8.74	6.62	12.61	11.95	12.42
	O	89.35	85.15	84.64	86.41	86.36	74.7	76.43	82.55	83.62	83.49
	Zn/Zr	---	0.03	0.17	0.48	0.70	1.89	2.56	0.38	0.37	0.33
b*	Zn	---	0.14	2.31	4.35	5.71	16.19	16.86	5.21	4.53	4.02
	Zr	22.4	27.25	25.98	19.08	17.81	18.71	14	24.74	24.37	24.91
	O	77.6	72.62	71.71	76.57	76.49	65.1	69.14	70.04	71.1	71.07
	Zn/Zr	---	0.01	0.09	0.23	0.32	0.87	1.20	0.21	0.19	0.16
c*	Zn	---	0.10	2.22	4.34	6.21	15.85	17.66	5.08	4.52	4.13
	Zr	32.35	38.84	36.59	27.48	25.07	26.36	20.6	33.74	33.66	33.96
	O	67.65	61.06	61.19	68.18	68.72	57.79	61.74	61.17	61.82	61.92
	Zn/Zr	---	0.00	0.06	0.16	0.25	0.60	0.86	0.15	0.13	0.12
d*	Zn	---	0.35	2.02	4.56	6.09	15.41	16.78	4.83	4.4	4.08
	Zr	40.97	40.03	43.96	34.51	30.98	32.09	25.3	41.23	40.37	41.88
	O	59.03	59.62	54.02	60.93	62.93	52.5	57.92	53.94	55.23	54.03
	Zn/Zr	---	0.01	0.05	0.13	0.20	0.48	0.66	0.12	0.11	0.10

* a, b, c, and d sets are measured at 5, 10, 15, and 20 kV electron beam energy, respectively.

Energy dispersive X-ray analysis (EDX) was employed to analyze the composition of the catalyst materials. The observed loading closely corresponds to the targeted values for the Zn/Zr ratio up to 0.28, as indicated in Table S1. However, at higher loadings, the detected amount of Zn on the catalysts near the surface exceeds the nominal values. This discrepancy is likely attributed to the separation of ZnO from the mixed oxide lattice, a finding supported by X-ray diffraction (XRD) and nitrogen physisorption results. Furthermore, the zinc concentration exhibits a decreasing trend as the voltage of the measurements increases. This suggests that zinc is less incorporated in the bulk of the metal oxide, indicating a surface enrichment of Zn.

Section 2. Raman spectroscopy

The phase assignment in the XRD profiles was confirmed by Raman spectroscopy (Fig. 2). Broad bands at 273, 467, and 652 cm^{-1} indicate the fluorite-like cubic structure [1] for $Zn_{0.19}ZrO_y$-500 and $Zn_{0.19}ZrO_y$-700, with the 467 cm^{-1} band corresponding to the Zr^{4+}-O stretch.[2] The band at 320 cm^{-1} is associated with a pseudo-cubic phase, where cations maintain a cubic structure while oxygen atoms undergo tetragonal distortion.[1] Upon calcination at 800 °C, the Raman spectrum changes considerably. New peaks corresponding to characteristic bands of the monoclinic and tetragonal phases dominate, centered respectively at 185, 192, 340, 386, 480, 566, 582, 615, 645 cm^{-1} and 227, 456, 506 cm^{-1}.[1–3]

Section 3. N_2 physisorption

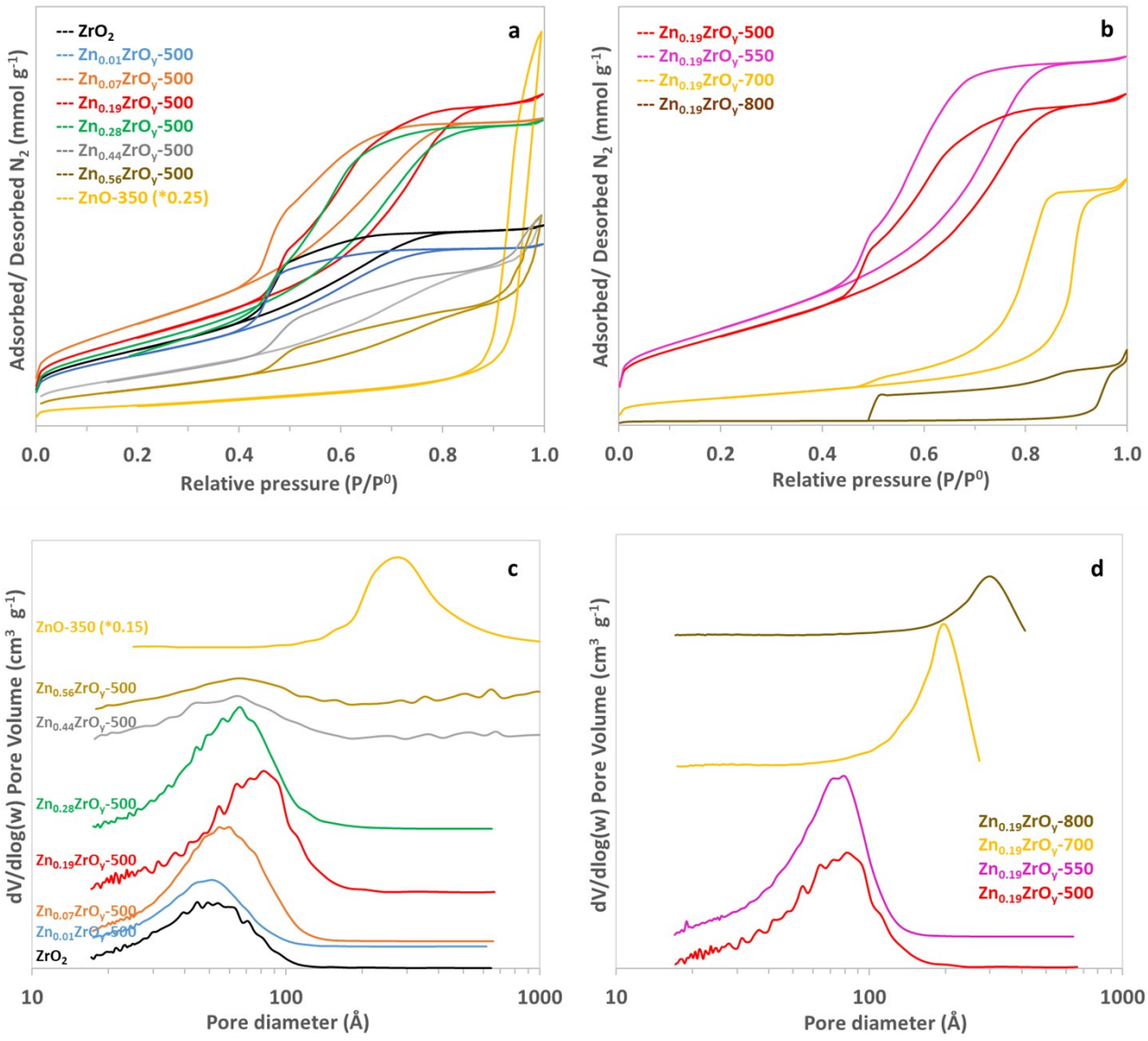

Fig. S1 N_2 adsorption-desorption isotherm of (a) Zn_xZrO_y-500 catalysts and (b) $Zn_{0.19}ZrO_y$-T calcined at 500, 550, 700, and 800 °C. Pore size distribution of (c) Zn_xZrO_y-500 catalysts and (d) $Zn_{0.19}ZrO_y$-T calcined at 500, 550, 700, and 800 °C.

Section 4. XPS

The Zr 3d spectra of ZrO_2 and $Zn_{0.19}ZrO_y$-800 were deconvoluted, considering the presence of both monoclinic and tetragonal phases, with a constant FWHM of 1.84 eV. Deconvolution of $Zn_{0.07}ZrO_y$-500, $Zn_{0.19}ZrO_y$-500, and $Zn_{0.19}ZrO_y$-700 XPS spectra with a constant FWHM of 1.84 eV revealed a peak at higher binding energies compared to the tetragonal phase, attributed to the formation of the cubic phase, and the emergence of a peak at 181.3 eV, assigned to Zn-O-Zr species. The broadening of the peaks in these samples was fitted with additional peaks at lower binding energies.

The Zn 2p spectra were deconvoluted considering the emergence of the Zn^{2+} peak at 1021.3 eV and keeping the FWHM constant at 2.0. The peak broadening at higher binding energies was fitted with a peak assigned to $Zn^{(2+\delta)+}$ species, while the peak broadening at lower binding energies was fitted with additional peaks attributed to $Zn^{(2-\delta)+}$ species.

Table S2. Details of the peak deconvolution of the Zn 2p, Zr 3d, and O 1s XPS spectra.

Catalyst	Zn $2p_{3/2}$				Zr $3d_{5/2}$					O 1s		
	$Zn^{(2-\delta)+}$	Zn^{2+}	Zn-O-Zr	$Zn^{(2+\delta)+}$	$Zr^{(4-\delta)+}$	Zr-O-Zn	Zr^{4+}- m	Zr^{4+}- t	Zr^{4+}- c	$O_{sublayer}$	$O_{lattice}$	$O_{chemisorbed\ surface}$
ZrO_2 (t-m)	---	---	---	---	27.3%	---	49.0%	23.6%	---	23.2%	52.5%	24.4%
$Zn_{0.07}Zr$-500 (c)	24.0%	46.8%	29.2%	---	16.1%	29.2%	---	---	54.7%	15.6%	58.7%	25.7%
$Zn_{0.19}Zr$-500 (c)	38.6%	26.3%	35.1%	---	34.7%	35.5%	---	---	29.8%	45.2%	40.2%	14.6%
$Zn_{0.19}Zr$-700 (c)	16.9%	27.1%	39.6%	16.4%	10.1%	40.9%	---	---	49.0%	16.8%	52.8%	30.3%
$Zn_{0.19}Zr$-800 (t-m)	43.6%	56.4%	---	---	---	---	---	34.5%	65.5%	24.6%	50.4%	25.0%

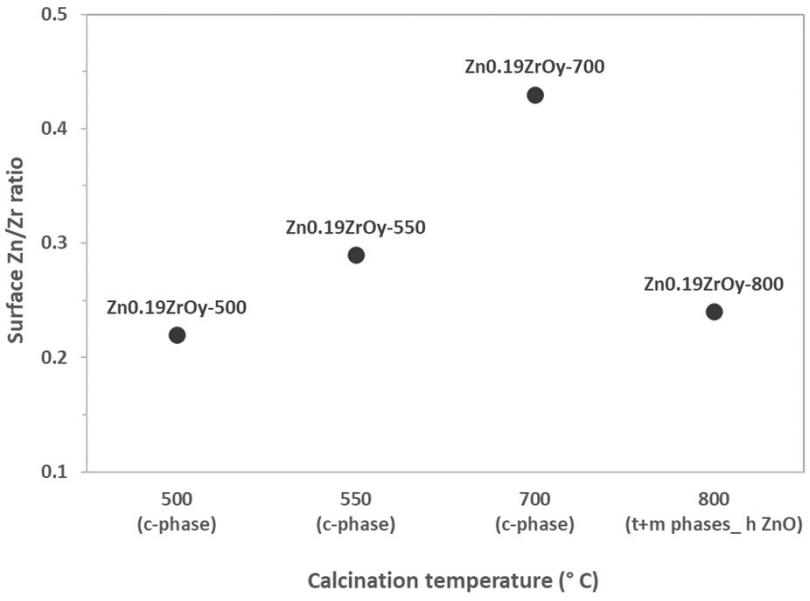

Fig. S2 Effect of calcination temperature on surface Zn/Zr ratio (from XPS).

The O 1s spectra are presented in Fig. S3, revealing spectral contributions at approximately 529-530 eV with two shoulders at lower and higher binding energies. The peaks observed at binding energies of 529-530 eV are identified as lattice oxygen ions (O^{2-}). In contrast, the peak at higher binding energy is attributed to weakly charged surface chemisorbed oxygen species, such as surface hydroxyl groups or oxygen vacancies.[4] The peak at lower binding energy (527.6 eV) can be assigned to physically adsorbed oxygen species[5] or oxygen atoms that are in subsurface layers (due to differences in their

chemical environment). The relative percentage of each oxygen component is summarized in Table S2. After Zn addition, the peaks shift to higher binding energies, representing the binding energy of O atoms in different crystal phases of ZrO_2. The emergence of low-energy O 1s species at 526.4 eV likely arises from the charge transfer between the neighboring O^{2-}, Zn^{2+}, and Zr^{4+} species [6] due to the formation of a mixed metal oxide.[5,7] Increasing the Zn/Zr ratio to 0.19 raises the ratio of low energy O 1s peaks while increasing the calcination temperature enhances the binding energy of the O 1s species.

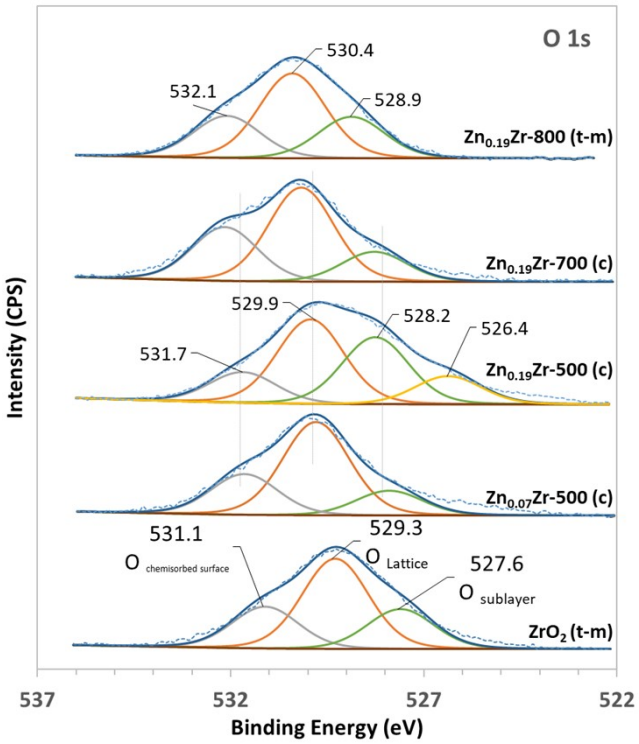

Fig. S3 Deconvoluted XPS spectra of O 1s in ZrO_2 (t + m), $Zn_{0.07}ZrO_y$-500 (c), $Zn_{0.19}ZrO_y$-500 (c), $Zn_{0.19}ZrO_y$-700 (c), and $Zn_{0.19}ZrO_y$-800 (t + m).

Section 5. CO_2-TPD

Table S3. Peak deconvolution of CO_2-TPD profiles.

		Peak 1	Peak 2	Peak 3	Total basicity
ZnO	T °C	122	347	412	
	CO_2 (μmol g^{-1})	0.54	0.22	0.83	1.59
	CO_2 (μmol m^{-2})	0.02	0.01	0.03	0.05
ZrO_2-500	T °C	104	159	280	
	CO_2 (μmol g^{-1})	3.29	3.84	6.83	13.96
	CO_2 (μmol m^{-2})	0.12	0.14	0.26	0.52
$Zn_{0.01}ZrO_y$-500	T °C	101	153	264	
	CO_2 (μmol g^{-1})	3.44	3.81	8.91	16.17
	CO_2 (μmol m^{-2})	0.13	0.14	0.34	0.61
$Zn_{0.07}ZrO_y$-500	T °C	109	160	250	
	CO_2 (μmol g^{-1})	5.68	4.92	12.71	23.31
	CO_2 (μmol m^{-2})	0.16	0.14	0.35	0.65
$Zn_{0.19}ZrO_y$-500	T °C	107	154	231	
	CO_2 (μmol g^{-1})	6.55	5.03	14.75	26.33
	CO_2 (μmol m^{-2})	0.21	0.16	0.47	0.84
$Zn_{0.28}ZrO_y$-500	T °C	113	162	248	
	CO_2 (μmol g^{-1})	9.46	8.43	26.60	44.48
	CO_2 (μmol m^{-2})	0.33	0.29	0.92	1.54
$Zn_{0.44}ZrO_y$-500	T °C	96	140	208	
	CO_2 (μmol g^{-1})	1.24	0.72	3.37	5.32
	CO_2 (μmol m^{-2})	0.07	0.04	0.19	0.30
$Zn_{0.56}ZrO_y$-500	T °C	112	162	260	
	CO_2 (μmol g^{-1})	0.94	0.91	1.91	3.76
	CO_2 (μmol m^{-2})	0.07	0.07	0.15	0.29
$Zn_{0.19}ZrO_y$-550	T °C	104	148	235	
	CO_2 (μmol g^{-1})	6.41	4.25	16.20	26.86
	CO_2 (μmol m^{-2})	0.19	0.13	0.48	0.79
$Zn_{0.19}ZrO_y$-700	T °C	104	151	263	
	CO_2 (μmol g^{-1})	8.64	7.57	21.68	37.88
	CO_2 (μmol m^{-2})	0.94	0.82	2.36	4.12
$Zn_{0.19}ZrO_y$-800	T °C	120	187	271	
	CO_2 (μmol g^{-1})	0.99	0.82	0.82	2.64
	CO_2 (μmol m^{-2})	0.90	0.75	0.75	2.40

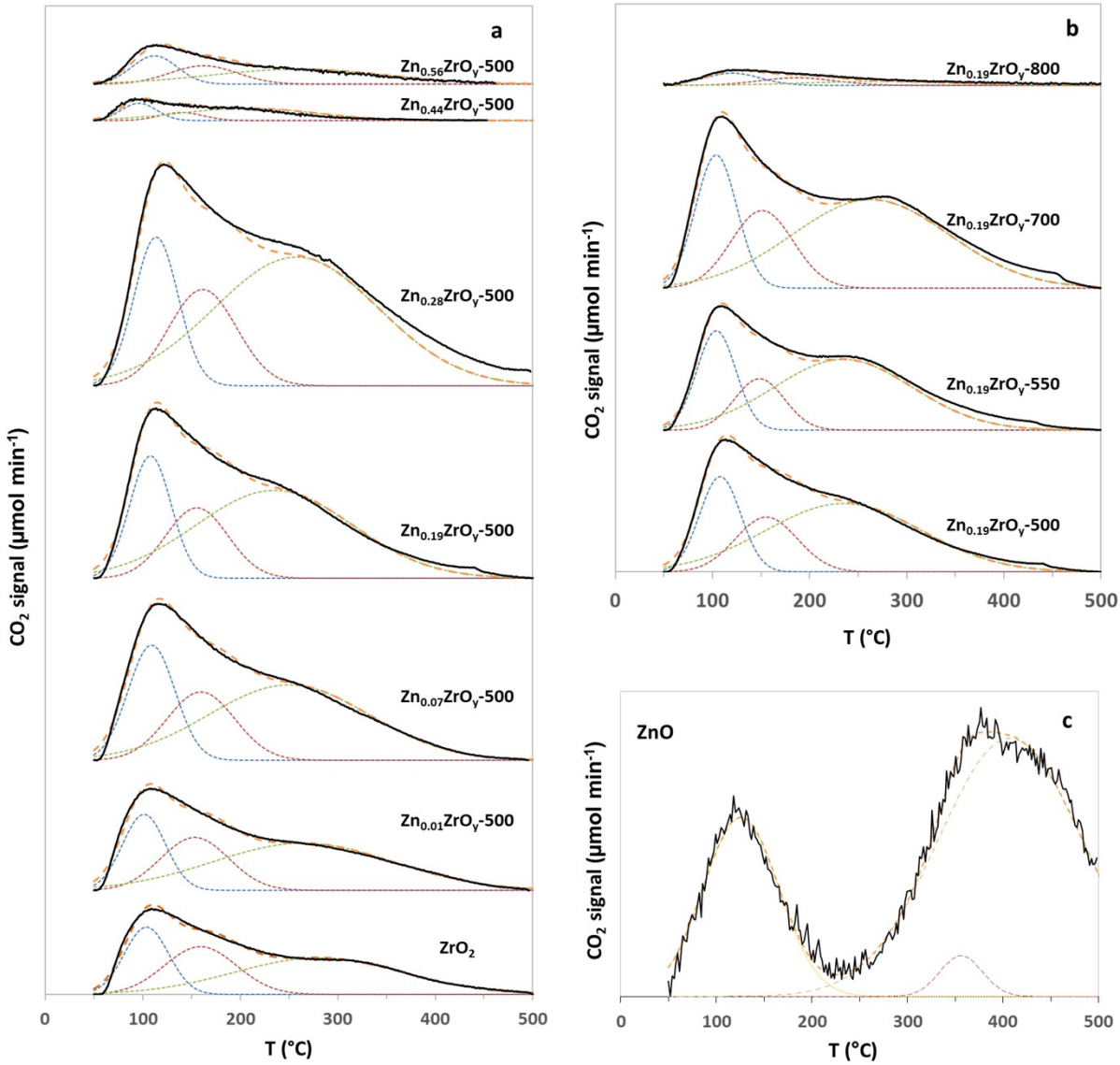

Fig. S4 Deconvolution of CO_2-TPD profiles of (a) Zn_xZrO_y-500 catalysts and (b) $Zn_{0.19}ZrO_y$-T calcined at 500, 550, 700, and 800 °C, and (c) ZnO. (Black full lines: measured data, dotted lines: deconvoluted data, and orange dash line: envelope)

Section 6. DRIFTS

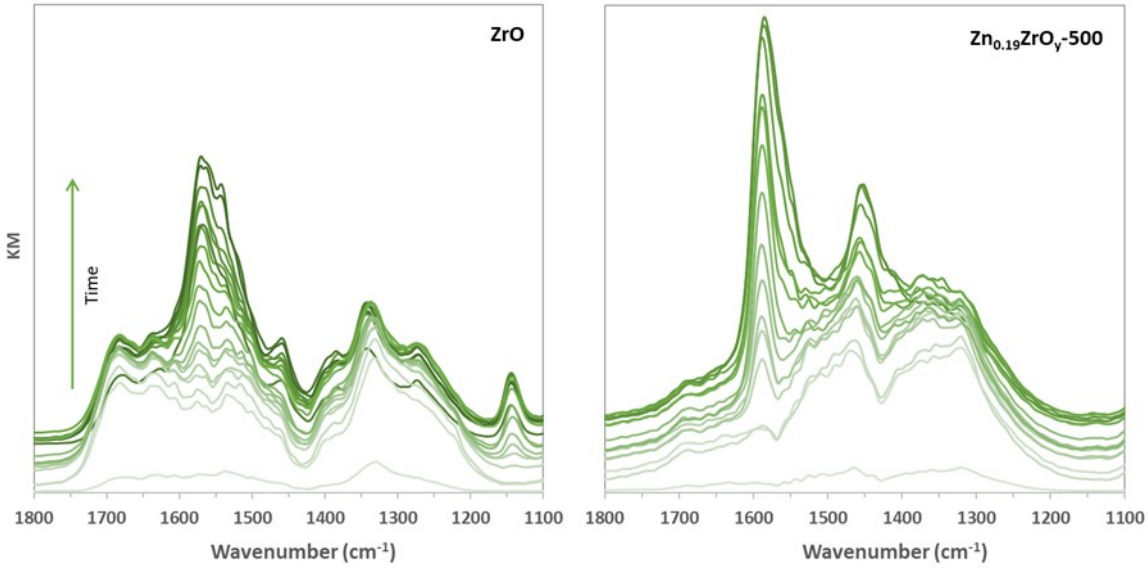

Fig. S5 Evolution of surface species during CO_2 adsorption on ZrO_2 and $Zn_{0.19}ZrO_y$ at 325 °C and 10 bar over 40 minutes.

Section 7. Zn_XZrO_y in literature

Table S4. Comparison of Zn_xZrO_y catalysts' performance in literature.

Catalyst	T, °C	P, bar	GHSV, ml g^{-1} h^{-1}	H_2:CO_2	CO_2 conversion, %	Methanol selectivity, %	Methanol STY, g g_{cat}^{-1} h^{-1}	reference
$Zn_{0.19}ZrO_y$	325	45	21000	3	4	82	0.20	This study
20%ZnO-ZrO_2	320	20	24000	4	4	82	0.20	[1]
$Zn_{0.2}ZrO_x$	320	50	24000	4	4	86	0.24	[2]
13%$ZnZrO_x$	320	20	24000	3	4	85	0.23	[3]
13%ZnO-ZrO_2	320	50	24000	3	10	86	0.50	[4]
ZnZr25	325	10	3600	3	8	40	0.04	[5]
15%ZnZr	300	40	12000	3	3	85	0.11	[6]
13%$ZnZrO_x$	320	50	24000	4	7	83	0.25	[7]
ZnO/ZrO_2-F *	320	30	24000	4	6	74	0.30	[8]
$ZnZrO_x$	330	45	10800	3	6	78	0.18	[9]
25%$ZnZrO_x$	350	30	4000	3	12	86	0.15	[10]

*hollow nano-frame

Section 8. Catalyst stability

The stability of the $Zn_{0.19}ZrO_y$-500 catalyst was assessed in CO_2 hydrogenation (Fig. S6). The effect of reaction temperature was studied by increasing the temperature from 350 °C to 400 °C, maintaining each temperature for 4 hours, and then decreasing the temperature back to 350 °C to determine if the same activity could be obtained. The result shows that the catalyst remains stable under these reaction conditions.

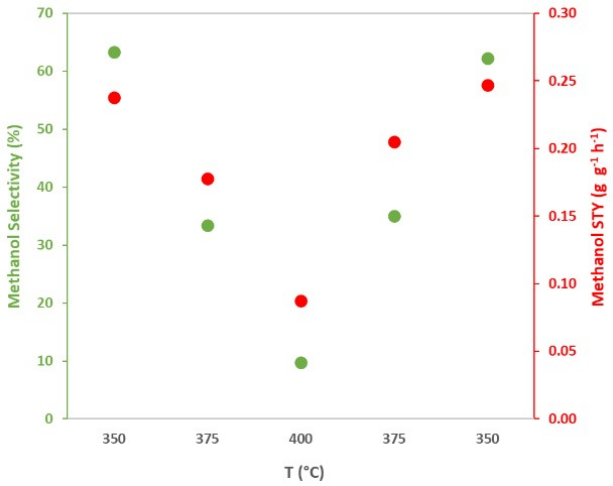

Fig. S6 Stability test of $Zn_{0.19}ZrO_y$-500 in CO_2 hydrogenation to methanol at 45 bar, H_2:CO_2:Ar=3:1:1, and GHSV= 21000 Nml g_{cat}^{-1} h^{-1}.

Section 9. Parameters correlation

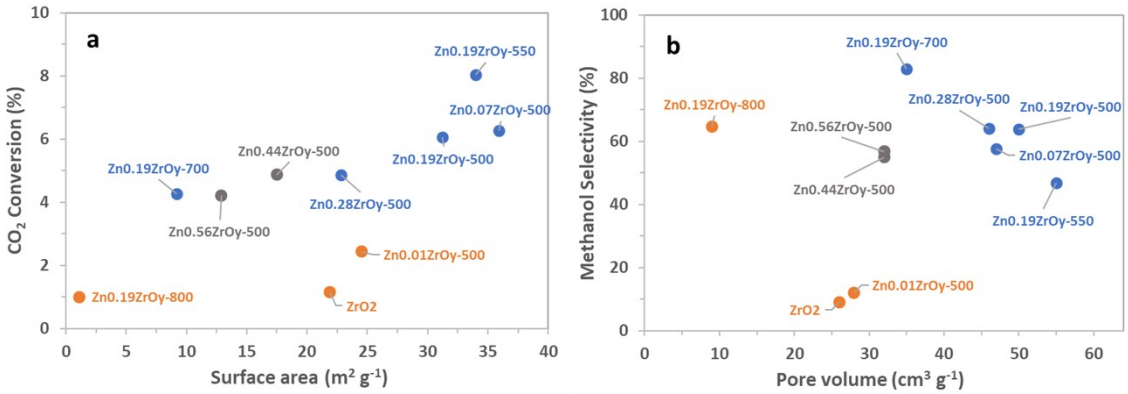

Fig. S7 Effect of (a) surface area on CO_2 conversion and (b) pore volume on methanol selectivity at 350 °C, 45 bar, H_2:CO_2:Ar=3:1:1, and GHSV= 21000 Nml g_{cat}^{-1} h^{-1} (blue colour: pure cubic-phase, grey colour: cubic-phase + h-ZnO, and orange colour: the rest of the samples).

Fig. S8 reveals the negative effect of ZnO formation on catalyst performance within the cubic-phase samples.

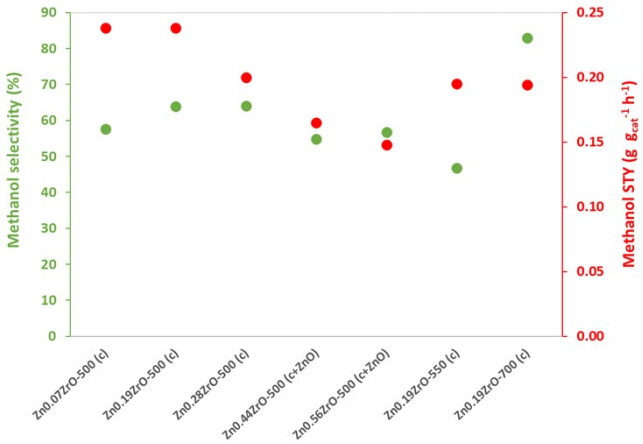

Fig. S8 Comparison of the performance of the cubic-phase catalysts at 350 °C, 45 bar, H_2:CO_2:Ar=3:1:1, and GHSV= 21000 Nml g_{cat}^{-1} h^{-1}.

The amount of CO_2 adsorption correlates with the surface Zn/Zr ratio (Fig. S9a). However, the increasing surface ratio of Zn/Zr and the consequently increased CO_2 adsorption do not directly relate to the methanol formation rate. Methanol formation peaks at a narrow Zn/Zr ratio of 0.18-0.22 and an adsorbed CO_2 range of 23.3-26.3 µmol g^{-1} (Fig. S9a and b).

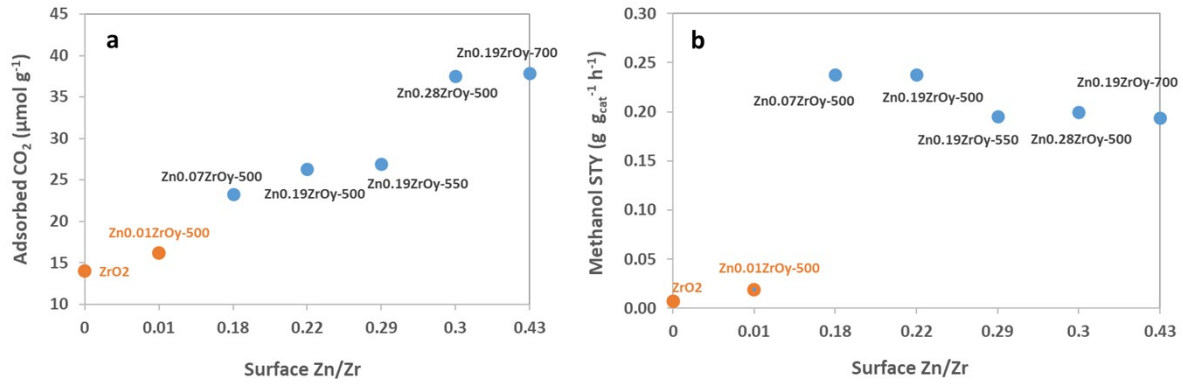

Fig. S9 Effect of surface Zn/Zr ratio on (a) CO_2 adsorption capacity, and (b) methanol formation at 350 °C, 45 bar, H_2:CO_2:Ar=3:1:1, and GHSV= 21000 Nml g_{cat}^{-1} h^{-1}.

References

1. Han, Z. *et al.* CO_2 hydrogenation to methanol on ZnO-ZrO_2 solid solution catalysts with ordered mesoporous structure. *Journal of Catalysis* **396**, 242–250 (2021).
2. Lee, K. *et al.* Atomic Pd-promoted $ZnZrO_x$ solid solution catalyst for CO_2 hydrogenation to methanol. *Applied Catalysis B: Environmental* **304**, (2022).
3. Feng, Z. *et al.* Asymmetric Sites on the $ZnZrO_x$ Catalyst for Promoting Formate Formation and Transformation in CO_2 Hydrogenation. *J. Am. Chem. Soc.* **145**, 12663–12672 (2023).
4. Wang, J. *et al.* A highly selective and stable ZnO-ZrO_2 solid solution catalyst for CO_2 hydrogenation to methanol. *Sci. Adv.* **3**, 1701290 (2017).
5. Tada, S. *et al.* Active Sites on $ZnZrO_x$ Solid Solution Catalysts for CO_2-to-Methanol Hydrogenation. *ACS Catalysis* **12**, 7748–7759 (2022).
6. Ticali, P. *et al.* CO_2 hydrogenation to methanol and hydrocarbons over bifunctional Zn-doped ZrO_2/zeolite catalysts. *Catalysis Science & Technology* **11**, 1249–1268 (2021).
7. Pinheiro Araújo, T. *et al.* Design of Flame-Made $ZnZrO_x$ Catalysts for Sustainable Methanol Synthesis from CO_2. *Adv. Energy Mater.* **13**, (2023).
8. Ren, Q. *et al.* Role of the structure and morphology of zirconia in ZnO/ZrO_2 catalyst for CO_2 hydrogenation to methanol. *Molecular Catalysis* **547**, 113280–113280 (2023).
9. Xu, D., Hong, X. & Liu, G. Highly dispersed metal doping to ZnZr oxide catalyst for CO_2 hydrogenation to methanol: Insight into hydrogen spillover. *Journal of Catalysis* **393**, 207–214 (2021).
10. Zhang, W. *et al.* Effective conversion of CO_2 into light olefins over a bifunctional catalyst consisting of La-modified $ZnZrO_x$ oxide and acidic zeolite. *Catal.Sci.Technol.* **12**, (2022).